Hydrogen Enhanced Localized Plasticity - A Mechanism For Hydrogen Related Fracture

H. K. Birnbaum and P. Sofronis*
Department of Materials Science and Engineering
*Department of Theoretical and Applied Mechanics
University of Illinois at Urbana-Champaign

ABSTRACT

The mechanisms of hydrogen related fracture are briefly reviewed and a few evaluative statements are made about the stress induced hydride formation, decohesion, and hydrogen enhanced localized plasticity mechanisms. A more complete discussion of the failure mechanism based on hydrogen enhanced dislocation mobility is presented and these observations are related to measurements of the macroscopic flow stress. The effects of hydrogen induced slip localization on the measured flow stress is discussed. A theory of hydrogen shielding of the interaction of dislocations with elastic stress centers is outlined. It is shown that this shielding effect can account for the observed hydrogen enhanced dislocation mobility.

REVIEW OF PERTINENT OBSERVATIONS

Despite extensive study, the mechanism(s) of hydrogen embrittlement has remained unclear. Several candidate mechanisms have evolved, each of which is supported by sets of experimental observations and strong personal views. One reasonable certain aspect of this controversy is that there are several viable mechanisms of hydrogen related failure and that the search for a single mechanism to explain all observations is doomed to failure. Of the many suggestions, three mechanisms appear to be viable; stress induced hydride formation and cleavage [1-4], hydrogen enhanced localized plasticity [5-9], and hydrogen induced decohesion [10,11]. The first of these has been definitively established to be operative in systems in which hydrides are either stable, or can be stabilized by the application of a stress field, e.g. Group Vb metals [3, 12-14], Ti [4. 15], and, Zr [16]. This "second phase mechanism is supported by microscopic observations [11, 17] and thermodynamic calculations [18]. In these hydride forming systems it has been shown [4] that under conditions in which the hydride cannot form, hydrogen "embrittlement" will occur by the second mechanism named above, hydrogen enhanced localized plasticity. The hydrogen enhanced localized plasticity mechanism is based on observations that in a range of temperatures and strain rates, the presence of hydrogen in solid solution decreases the barriers to dislocation motion, thereby increasing the amount of deformation that occurs in a localized region adjacent to the fracture surface [19-25]. The fracture process is a highly localized plastic failure process rather than an embrittlement. This counterintuitive process says that the macroscopic ductility is limited by the onset of extensive localized plasticity and is supported by microscopic

observations. The third viable mechanism is the hydrogen related decohesion mechanism in which the atomic bonding at the crack tip is weakened by the presence of hydrogen in solid solution [10,11]. This mechanism is supported primarily by the observations that in some non-hydride forming systems, hydrogen embrittlement appears to occur in the absence of significant local deformation, by theoretical calculations of the effect of hydrogen on the atomic potentials [26] and by a thermodynamic argument [27, 28]. Direct evidence for this mechanism has not been obtained and measurements which have been made on the effects of hydrogen on small strain aspects of the lattice potential suggest no softening of the lattice potential [7].

In the present paper we will review the observations supporting the hydrogen enhanced localized plasticity (HELP) mechanism of hydrogen embrittlement and then discuss the mechanism by which hydrogen enhances the mobility of dislocations. Experiments on which the HELP mechanism is based are founded on the premise that detailed understanding of fracture mechanisms requires observations at sufficiently high resolution to allow the mechanistic details to be revealed. High resolution fractography of hydrogen embrittled metals, such as Ni and Fe, show extensive plastic deformation localized along the fracture surfaces [25, 29]. Particularly revealing results have been obtained with the technique of *in situ* environmental cell deformation and fracture. These methods allow observation of the fracture process in real time, at high spatial resolution, and in vacuum or in H_2 atmospheres. These studies have been carried out for bcc, fcc, and hcp metals having various solute contents and for solid solutions, precipitation strengthened alloys, and intermetallics [19-24, 30]. In systems which exhibit hydrogen embrittlement, the nature of hydrogen effects, while differing in details, were the same in fundamental character.

The most dramatic observation was that hydrogen increased the dislocation mobility under conditions of constant stress. In stressed specimens, dislocation mobility could be increased by the addition of H_2 to the environmental cell and decreased by removal of H_2 and restoration of vacuum. This behavior was observed for edge, screw, and mixed dislocations and for isolated dislocations as well as dislocation tangles. In bcc metals the enhanced dislocation velocities were observed on {112} and {110} slip planes and the enhancement was least for extremely high purity Fe and increased as interstitial solutes (C) were added to the solid solution. Hydrogen enhanced dislocation velocity was observed for dislocations completely contained within the specimens as for Frank-Read sources and for dislocations which terminated at the surfaces. Hydrogen enhanced operation of dislocation sources were observed within the crystals and at grain boundaries.

Specimens which contained stress concentrations, such as notches, failed by ductile plastic processes at the front of the notch when stressed in Mode 1 in vacuum. When stressed under gaseous H_2, similar fracture was observed, with the exception that the extent of plasticity was more confined to regions adjacent to the fracture surface in the case of fracture in H_2. In relatively pure specimens (Ni. Fe, etc.) the

fracture tended to be along slip planes and the deformation accompanying the fracture in H_2 was within 1 micrometer of the active slip plane. In alloys such as stainless steels [23], the fracture in H_2 was much less crystallographic and tended to be along the plane of maximum normal stress.

In all of the systems, the cracks which had propagated in vacuum and then stopped under a constant external load could be started and continued to propagate without any increase in external load when H_2 was added to the environmental cell. This process occurred by increasing the dislocation activity at the crack tip when the specimen was exposed to H_2 gas. Since the fracture process in H_2 was by localized ductile failure e.g. by the formation of very shallow, localized microvoids [31], the increase in the dislocation velocity at the crack tip is the root cause of the hydrogen embrittlement. The effect of hydrogen is greatest at the crack tip where either hydrogen entry is facilitated by slip processes or the local hydrogen concentration is increased by the effect of stress on the chemical potential of the solute H. Hydrogen locally softens the material in front of the crack allowing ductile fracture to occur there, prior to general yielding away from the crack tip. In the cases where the concentration of hydrogen is greatest in the vicinity of grain boundaries [32-34], it is in these regions that deformation occurs at the lowest stresses and hence "intergranular" fracture is observed. In cases where high resolution studies of these "intergranular" fracture have been carried out [4, 35] it is clear that the fracture in fact occurs by plastic processes in the vicinity of the boundaries rather than along the boundaries themselves.

HYDROGEN EFFECTS ON MACROSCOPIC DEFORMATION

Despite the many observations of hydrogen enhanced dislocation mobility in TEM specimens, relatively few observations of softening due to hydrogen in solid solution have been reported. In most cases, the introduction of hydrogen has been reported to result in increased flow stress and only in a small number of cases has softening been observed [36-39]. Significant decreases of the flow stress have been reported in high purity iron which was cathodically charged at very low current densities and during hydrogen charging under conditions in which the hydrogen was introduced without damage to the specimen. Two significant differences appear to divide the experiments which exhibit softening due to hydrogen from those which do not. Hydrogen decreases have been observed at very low strain rates and when hydrogen was introduced under conditions which did not cause any structural damage to the specimens. The latter condition is particularly significant, as most cathodic charging conditions used to introduce high supersaturations of hydrogen introduce high concentration gradients and correspondingly high stresses near the surface. The consequent deformation in the near surface region gives rise to hardening which may mask the softening caused by hydrogen. In the case of the cathodic charging conditions utilized by Kimura et al [36-38], no surface deformation was observed.

The effects of hydrogen on the thermal activation of dislocations over barriers has been studied using the techniques of load relaxation, temperature and strain rate changes in high purity Ni and Ni-C alloys [40]. The strain rate can be expressed as:

$$\dot{\varepsilon} = \dot{\varepsilon}_o \exp -\left[\left(\Delta H_o^* - \int bA^* \delta\sigma^*\right) / kT\right] \qquad (1)$$

where $\dot{\varepsilon}_o$ is a constant which is given by $\dot{\varepsilon}_o = \nu_D \rho_m A \exp(\Delta S^* / k)$, ν_D is the dislocation attempt frequency, A is the slip plane area swept by the dislocation per activated event, ΔS^* is the activation entropy for slip activation, ΔH_o^* is the activation enthalpy for slip activation at zero stress, A^* is the activation area, b is the Burgers vector, and σ^* is the effective stress. The measured activation parameters are related to the dislocation velocity by:

$$v_D = \left(\dot{\varepsilon}_o / \rho_m b\right) \exp -\left(\Delta H^* / kT\right) \qquad (2)$$

where $\Delta H^* = \Delta H_o^* - \int bA^* \delta\sigma^*$ The critical parameters which control the thermal activation of dislocations over barriers are the activation volume, A^*, and the activation enthalpy, ΔH^*. These parameters were determined using stress relaxation and temperature cycling techniques on Ni and Ni-C alloys [40].

The results of these measurements are shown in Figs. 1 and 2. As expected from the strong strengthening effects of C in solid solution in Ni, solute C increases A^* over a wide stress range and increases ΔH^* over the same stress range. This is consistent with C solutes or small C clusters causing strong barriers to the dislocation motion. In contrast, solute H decreases A^* and decreases ΔH^* consistent with a hydrogen related decrease in the strength of the dislocation obstacles. Adding hydrogen solutes to a Ni-C alloy has the effect of approximately removing the increased v^* and H^* caused by C, i.e. removing the enhanced dislocation obstacles caused by C. Using Eqn. 2, these results can be used to calculate the effects of solute H on dislocation velocities with the results shown in Table 1 where σ_a is the applied stress, $\delta\Delta H^*$ is the hydrogen induced change in activation enthalpy, $\delta A^*/b^2$ is the hydrogen induced change in activation area, and v_D^H / v_D is the dislocation velocity in the presence of H relative to that in the absence of H as calculated from the measured dislocation parameters.

The values of v_D^H / v_D indicate that significant enhancement of the dislocation velocities are expected in Ni-H and Ni-C-H alloys, particularly at the lower applied stresses. This is in accord with the *in situ* TEM studies in which the stresses, while not directly measured, are expected to be in the range of 100-150 MPa. These results indicate that the H related softening is greatest at the lower applied stresses where the dislocation velocities are the smallest.

Table 1. EFFECT OF HYDROGEN ON THE ACTIVATION ENTHALPY, ACTIVATION AREA AND DISLOCATION VELOCITY

	σ_a (MPa)	$\delta\Delta H^*$ (eV)	$\delta A^*/b^2$	v_D^H / v_D
Pure Ni	50	-0.32	-500	3×10^5
Pure Ni	100	-0.11	-200	81
Pure Ni	150	-0.05	-100	7
Ni-C	50	-0.49	-800	3×10^8
Ni-C	100	-0.13	-300	181
Ni-C	150	-0.06	-150	11

SLIP LOCALIZATION

Measurements of H induced changes in the dislocation activation parameters using stress relaxation and thermal cycling measurements, were carried out on bulk specimens. While they have not been carried out on as wide a range of materials as the TEM studies, they indicate that the *in situ* TEM studies are not artifacts of the use of thin specimens. There does remain the question of why many studies, which measure macroscopic stress-strain curves, exhibit increases in the measured flow stresses due to the introduction of hydrogen, whereas the TEM specimens generally show either no effect (in materials which do not absorb significant amounts of hydrogen) or an enhanced dislocation velocity due to the introduction of hydrogen. One factor, discussed briefly above, is the introduction of near surface damage due to the H charging of macroscopic specimens, which would cause hardening in a flow stress determination. This damage, which results from the severe hydrogen concentration gradients (and accompanying stress gradients) which can often accompany cathodic charging, will depend on the details of the charging conditions, the surface condition, and the purity of the material (through the propensity for impurities to trap hydrogen, decrease the diffusivity and increase the near surface concentration gradients).

Another factor is the localization of slip on a limited number of slip planes due to hydrogen charging as observed in stainless steels [41], Ni [42], and high purity Al [39]. In the stainless steel-H alloys the strain localization was accompanied by significant increases in the flow stress, while in the Al-H alloys, significant decreases in the flow stresses was observed. Shear localization occurs if the flow stress in the region of localization is reduced relative to the flow stress of the non-deforming volume. This can occur in several ways and a number of these cases are considered below.

Case I. In systems where H reduces the barriers to dislocation motion, an inhomogeneous distribution of H can cause shear localization since the flow stress

is lower where the H concentration is greatest. This may occur if H entry is facilitated at slip line intersections with the surface.

Case II. Shear localization can occur when the specimen is hardened by the introduction of hydrogen (due to the formation of hydrides or H clusters), if the initial deformation locally reduces the stress for continued slip. This is believed to be the case for the Al-H system where the hardening of the crystal is believed to occur by the formation of small hydrogen clusters [43]. Removal of these clusters during the initial passage of dislocations leads to slip localization as in other precipitation hardened systems.

Increases in dislocation mobility due to the presence of solute H will enhance this slip localization in both cases. The macroscopic flow stress can be increased or decreased, depending on the magnitude of the local softening due to the removal of dislocation barriers. In the case of stainless steel, severe slip localization is accompanied by significant increases in the macroscopic flow stress [41] while in the case of Al the macroscopic flow stress is reduced [39].

In a tensile test, the usual assumption is that the deformation occurs relatively uniformly over the gage length, l. The tensile machine imposes a deflection rate, $\dot{l}$, and the specimen responds by deformation at a strain rate, $\dot{\varepsilon}$, defined as $\dot{l}/l_0$ or $d(\ln(l/l_0))/dt$. The response function of the specimen is the flow stress, τ_f. The strain rate is related to the dislocation parameters by:

$$\dot{\varepsilon} = \rho_m b v_0 \tau_f^m \qquad (3)$$

where b is the Burgers vector, ρ_m is the mobile dislocation density, τ_f is the resolved shear stress, m is a material dependent exponent having values between 1 and about 30, and v_0 is a material constant.

In the absence of any effect of H on the dislocation properties, The ratio of the flow stress for the specimen undergoing shear localization, τ_l, to one which is uniformly deforming, τ_u is given by:

$$\tau_l / \tau_u = \left(l_u / l_l \right)^{1/m} \qquad (4)$$

where l_l/l_u is the fraction of the gage length in which localized shear occurs. The parameter l_l/l_u can be approximated by the ratio of the slip line density in the specimen exhibiting localized slip and that which exhibits uniform slip. Values for the increased measured flow stress due to shear localization in the absence of any H related increases in dislocation mobility are given in Table II for a range of l_l/l_u and m.

As seen in Table II, significant hardening can occur with relatively moderate shear localization. Hence if H causes shear localization and no enhanced dislocation velocity, as has been observed, the macroscopic flow stress will increase; a reflection of the slip distribution rather than the effects of H on dislocation behavior.

Table II INCREASED FLOW STRESSES DUE TO SHEAR LOCALIZATION IN THE ABSENCE OF HYDROGEN SOFTENING

l_u / l_l	τ_l / τ_u			
	m = 1	m = 5	m = 10	m = 30
10	10	1.58	1.26	1.08
10^2	10^2	2.51	1.59	1.17
10^3	10^3	3.98	2.00	1.26
10^4	10^4	6.31	2.51	1.36

If H alters the dislocation response to an applied stress, the effects of shear localization on the measured flow stress is somewhat more complex. The measured flow stress, τ, can be written:

$$\tau = \left[\frac{\dot{l}}{\rho_m b v_o l_o} \right]^{1/m} . \qquad (5)$$

Since the displacement rate ($\dot{l}$) is set by the testing machine, the ratio of the flow stress with and without H is written:

$$\frac{\tau_H}{\tau} = \frac{[\rho_m v_o]^{1/m}}{[\rho_{m,H} v_{o,H}]^{1/m_H}} \qquad (6)$$

where the subscript H indicates the value in the presence of H. In the presence of <u>both</u> shear localization and hydrogen effects on dislocation mobility, the flow stress ratio can be written:

$$\frac{\tau_{H,l}}{\tau} = \left[\frac{\tau_l}{\tau_u} \right] \left[\frac{\tau_H}{\tau} \right] = \left[\frac{l_u}{l_l} \right] \left[\frac{(\rho_m v_o)^{1/m}}{(\rho_{m,H} v_{o,H})^{1/m_H}} \right] \qquad (7)$$

where $\tau_{H,l}$ is the flow stress in the presence of H and slip localization. The parameters necessary to discuss these equations in detail have not been measured as a function of H concentration. It is evident however, that the measured flow stress can either be increased or decreased by the presence of H depending on the extent of shear localization, (τ_l/τ_u), and the effect of H on the dislocation mobility, (τ_H/τ). Thus measurement of the effects of H on the macroscopic flow stress alone is not a reliable means of determining dislocation behavior. Measurements of the macroscopic stress strain behavior which show <u>increases</u> in the flow stress due to

the introduction of H may result from shear localization even in the presence of reduced barriers to dislocation motion.

The *in situ* TEM observations suggest that the introduction of H increases ρ_m as well as the velocities of individual dislocations. Increases in dislocation velocity due to H suggests that both m_H and $v_{o,H}$ are increased by the H solutes. From Eqn. 7:

macroscopic hardening is expected for $$\left(\frac{l_u}{l_l}\right) > \left(\frac{\left[\rho_{m,H} v_{o,H}\right]^{m/m_H}}{\rho_m v_o}\right)$$

and softening is expected for $$\left(\frac{l_u}{l_l}\right) < \left(\frac{\left[\rho_{m,H} v_{o,H}\right]^{m/m_H}}{\rho_m v_o}\right).$$

ELASTIC SHIELDING OF STRESS CENTERS

Since the hydrogen related softening was observed in fcc, bcc, and hcp systems, in pure metals, solid solutions, and in precipitation hardened systems, it appears to be a very general effect. Hence the cause for this softening should be sought in the elastic interactions between dislocation and between dislocations and other stress centers, such as solute atoms and precipitates. It is this elastic interaction which provides the common strengthening mechanism in all these systems. Hydrogen atmospheres form in the dilatational fields of the elastic singularities; in the tension field of the edge dislocations, in the volume surrounding solutes (in particular interstitial solutes), and in the vicinity of precipitates. The primary cause of the interaction which gives rise to the H atmospheres is the first order dilatational interaction energy, W_{int} which can be expressed as:

$$W_{int} = -\frac{1}{3}\sigma^a_{kk}\Delta v \qquad (8)$$

where σ^a_{kk} is the stress field of a defect and Δv is the unconstrained volume dilatation of the H solute. For the interaction of H with an edge dislocation this may be written:

$$W_{int} = -\frac{\mu b(1+\upsilon)\sin\phi}{3\pi(1-\upsilon)r}\Delta v \qquad (9)$$

where μ and ν are the shear modulus and Poisson's ratio respectively, b is the magnitude of the Burgers vector, and ϕ and r are the polar coordinates as measured from the dislocation core and slip plane. As a result of this elastic interaction, the concentration of H in the atmosphere is described by [44]:

$$\frac{c_H}{1-c_H} = \frac{c_o}{1-c_o}\exp\left(-\frac{W_{int}}{kT}\right) \qquad (10)$$

where c_o is the H concentration far from the defect in a zero stress field, and c_H is the H concentration in the atmosphere. In addition to this first order elastic interaction,

there is a second order elastic interaction energy which arises from the change in the elastic moduli caused by the presence of H in solid solution. For the case of the Nb-H system:

$$\mu = \mu_o \frac{1+0.34c_H}{1-0.0177c_H}, \quad \upsilon = \upsilon_o - 0.025c_H, \quad E = E_o(1+0.34c_H). \tag{11}$$

The second order elastic interaction between H and the dislocation may be written as:

$$W'_{int} = \frac{1}{2}\varepsilon_{ij}\varepsilon_{kl}\left(c'_{ijkl} - c_{ijkl}\right) \tag{12}$$

where the primed elastic constants refer to those in the presence of H in solid solution.

The effects of H on the elastic interactions between defects have been calculated using a linear elasticity and finite element techniques [45] and some of the results are summarized below. Shielding of the elastic interactions results from the fact that the hydrogen atmospheres around both the dislocation and the interacting stress centers respond to the total stress at each point. The total elastic force between the defects must include the interaction forces between the dislocation and the elastic center, between the H atmospheres, and between the H atmospheres and the dislocation and elastic stress center.

In the absence of hydrogen, the interaction force per unit length between two parallel dislocations is given by:

$$\mathbf{F} = \sigma_1 \mathbf{b}_2 \times \xi \tag{13}$$

where $\boldsymbol{\sigma}_1$ is the stress tensor of dislocation 1, $\mathbf{b}_i$ with i=1,2, are the Burgers vectors, and ξ is the unit vector along the dislocation lines. In component form, Eqn. 13 is written as $F_i = \varepsilon_{ijk}(\sigma_1)_{jm}(b_2)_m\xi_k$ where ε_{ijk} is the alternating symbol. In the case to be discussed, parallel edge dislocations, Eqn. 13 results in a repulsive force if the dislocations are of the same sign and on the same slip system. In this case, the force on dislocation 2 due to dislocation 1 is $\tau_D b_2$ where τ_D is the stress of dislocation 1 resolved along the slip plane and Burgers vector.

The hydrogen effect on the interaction between the dislocations 1 and 2 (Fig. 3) is assessed by calculating the hydrogen induced change in the shear stress τ_D due to interactions between the hydrogen atmospheres surrounding the two dislocations. These hydrogen atmosphere are modeled by a continuous distribution of dilatation lines parallel to the dislocation lines. Each dilatation line is viewed as a stress source which affects the shear stress τ_D. This type of model for the hydrogen effect is consistent with the plane strain assumption for the dislocation strain field when the hydrogen concentration does not vary in the direction of the dislocation lines. In that case the in-plane concentration of the dilatation lines, n, is directly related to the hydrogen concentration per unit volume, C through n=Ch where h is the distance between two successive hydrogen atoms along the dilatation line and the

concentration n denotes the number of hydrogen atoms per unit area in the plane normal to the dilatation line.

The net shear stress, τ_H, induced by the hydrogen atmospheres is found by integration of the stress contributions of each of the H dilatation lines over the entire area S occupied by the atmosphere. In polar coordinates, the shear stress on dislocation 2 due to the H atmospheres is given by:

$$\tau_H = -\frac{\mu}{2\pi(1-\nu)}\frac{V_H}{N_A}\int_0^{2\pi} C(r,\phi)\frac{\sin 2\phi}{r}drd\phi \qquad (14)$$

where r_2 is the inner cutoff radius of dislocation 2 and R is the outer cutoff radius of the atmosphere centered at dislocation 2. The core of dislocation 1 with cutoff radius r_1 is also excluded from the integration. The elastic solution shows that the stress field of a hydrogen dilatation line is purely deviatoric. Consequently, the interaction energy between the hydrogen dilatation lines is zero and introduction of a dilatation line into the lattice is energetically independent of the presence of the neighboring lines. Therefore the hydrogen concentration $C(r,\phi)$ at any position (r,ϕ) is determined solely by the corresponding stress due to dislocations 1 and 2. Superposition of the singular linear elastic stress fields of the two dislocations yields the in-plane hydrostatic stress as:

$$\frac{\sigma_{11}^a + \sigma_{22}^a}{2} = -\frac{\mu}{2\pi(1-\nu)}\left(b_2\frac{\sin\phi}{r} + b_1\frac{r\sin\phi - l\sin\omega}{r^2 + l^2 - 2rl\cos(\phi-\omega)}\right) \qquad (15)$$

where l and ω are the polar coordinates of the position of dislocation 1 (see Fig. 3). Then concentration $C(r,\phi)$ at every point in the solid is calculated using the total stress field, Eqn. 15.

Equation 14 indicates that the stress field of a hydrogen dilatation line decays as $1/r^2$ with distance r. It is expected that the magnitude of the shear stress due to H, τ_H, will depend mainly on the dilatation lines close to the core of dislocation 2. The corresponding shear stress, τ_D, at the core of dislocation 2 due to dislocation 1 is given by

$$\tau_D = -\frac{\mu b_1}{2\pi(1-\nu)}\frac{\cos\omega\cos 2\omega}{l} \qquad (16)$$

and the net shear stress exerted on dislocation 2 is equal to $\tau_D + \tau_H$.

Calculations of hydrogen effects on the dislocation interactions were carried out using the parameters appropriate to Nb, as there is a full set of data available for the Nb-H system. The hydrogen atmosphere in equilibrium with the stress field of a single dislocation in an infinite medium is shown in the form of normalized iso-

concentration lines, C/C_o, in Fig. 4 at a nominal concentration C_o=0.1 hydrogen atoms per solvent atom and a temperature of 300K. The atmosphere is symmetric with respect to the dislocation plane because of the corresponding symmetry in the hydrostatic stress field of the dislocation. Under the same temperature and nominal hydrogen concentration, Figs. 5 and 6 show the hydrogen atmosphere for dislocations 1 and 2 on the same slip system and at respective relative positions of 10, 8 and 6 Burgers vectors apart. In Fig. 6 the Burgers vector of dislocation 2 is negative. The portion of the hydrogen atmosphere round each dislocation is non-symmetric when compared with the atmosphere of the single dislocation shown in Fig. 4 as a direct result of the linear superposition in the stress field of the two dislocations. For dislocations of the same sign, the hydrostatic stress field is reinforced positively below the slip plane and negatively above the slip plane. For any given point in the area between the dislocations this reinforcement increases as the dislocations approach each other. Consequently the hydrogen concentration increases in the regions of positive stress enhancement and its value becomes larger than the concentration of the corresponding region in the atmosphere of a single dislocation. In contrast, the positive hydrostatic stress field of each dislocation is weakened in the case of dislocations of opposite sign. As a result, the level of hydrogen accumulation in the tensile regions of the two dislocations is lower that of a single dislocation alone.

In Figs. 7 and 8 the hydrogen induced shear stress, τ_H, at the core on the slip plane of dislocation 2 is plotted against distance l between the dislocations at H/m= 0.1, 0.01 and 0.001 and at a temperature of 300K. The angle ω is equal to 180° (see Fig. 3) and in Fig. 8, dislocation 2 has a negative Burgers vector. The shear stress is normalized by the shear modulus μ and the distance by the Burgers vector magnitude b. In the same figures the normalized shear stress, τ_D/μ, due to dislocation 1 in the absence of hydrogen and the total normalized shear stress, $(\tau_D+\tau_H)/\mu$, are plotted as well.

The shear stress on dislocation 2, due to hydrogen, is negative and its absolute value increases as the nominal H concentration, c_o, becomes larger, consistent with concentration dependence of the H line density. In both the interactions between like signed dislocations and unlike signed dislocations the effect of hydrogen is to decrease the force exerted on dislocation 2 by dislocation 1.

The effects of hydrogen shielding on the interaction of edge and screw dislocation with solutes having lower symmetry that the lattice, e.g., interstitials in bcc metals [46], have been calculated using a finite element method in a self consistent procedure which minimizes the energy of the system while calculating the H distribution around the dislocation and the solute atom. In the absence of H, the method gives good agreement with the analytic calculations of Cochardt et al [46]. In the presence of H, the complete elastic solution is satisfied with variable moduli which depend on the local H concentration. The results of these calculations for the interactions of an edge dislocation lying along the [211], with its Burgers vector in the $[1\bar{1}1]$, with C interstitials having their tetragonal axes along the three <100> are

shown in Figs. 9-11. The analytic result is in good agreement with the previous calculations [46] and the effect of H in solid solution is to markedly decrease the interaction energy for all three C orientations. For all three C orientations, the presence of H causes a decrease in the edge dislocation - C interaction energy of about 0.5 eV. The decrease in the interaction energy with H is consistent with the measured decrease in the activation enthalpy, ΔH^*, for thermally activated deformation [40]. Similarly, the presence of H gives rise to a decrease in the width of the interaction potential well which is consistent with the measured decrease in the activation area, A^*, in the presence of solute H as determined by the thermally activated flow measurements [40].

DISCUSSION

The consequence of hydrogen shielding of the stress fields of elastic singularities are numerous and will be explored in a subsequent publications. At the present time, we wish simply to point out some of the situations which will be of greatest interest for the issues of hydrogen related fracture. In all cases, the shielding effects are manifested at low strain rates and at temperatures where the H solutes retain a high mobility. In the absence of hydrogen, it is well known that two parallel edge dislocations on the same slip system and with Burgers vectors of the same sign repel each other. Both the analytical and finite element calculation of H shielding indicate that the shielding greatly reduces the repulsive force acting between the dislocations on the glide plane. This reduction is associated with the volumetric strain produced by the introduction of hydrogen into the lattice, (volumetric effect), and the hydrogen induced changes in the constitutive moduli, (modulus effect). The hydrogen related decrease of the repulsive interaction depends strongly on the nominal hydrogen concentration, as indicated by Fig 7. As expected from the fact that the H shielding effect results from the stress fields of point defects, it affects the interaction between dislocations at short range, in agreement with the $1/r^2$ dependence of the stress field of the interstitial hydrogen. At sufficiently high H concentrations, the repulsive stress field at short range can become attractive due to the H stress fields, possibly leading to coalescence of the leading dislocations at the head of a pileup and the formation of a crack in the manner suggested by Stroh [47]. A similar reduction of the attractive force between opposite signed dislocations leads to a weakening of the slip barriers provided by dislocation dipoles. Similarly, the forces acting on dislocations which cause glide polygonization are decreased by the presence of solute H atmospheres, leading to a more random dislocation distribution during deformation and to a lowering of the internal stress fields.

The most significant effect seems to be a decrease in the strength of the interactions between dislocations and point defects and between dislocations and internal stress fields provided by other dislocations due to the H shielding, as shown in Figs. 7-11. Both of these leads to an increased dislocation velocity under stress as the slip barriers can be more easily overcome by thermal activation. These effects are shown schematically in Fig. 12 for various temperatures and strain rates. The effects of solute H are expected to be small at elevated temperatures where no significant H

atmospheres can form at the dislocations or at the barriers to slip. "High temperature" behavior is expected when kT > B, the "binding enthalpy" of H to the dislocation. Since the effects of H shielding are manifest only if the H atmospheres can move with the dislocations, little effects due to shielding are expected at "low temperatures". The definition of "low temperature" depends on the dislocation velocity and hence the imposed strain rate and mobile dislocation density. In the "low temperature" range a small yield point may be expected as the pinning of the dislocations by the immobile H atmospheres limits the initial mobile dislocation density and allows the dislocations to exhibit "breakaway effects". Both decreases and increases in dislocation velocities due to H atmospheres can be manifested at "intermediate temperatures" where the H can move with the dislocations. At high strain rates, where the H atmospheres move with, but lag behind the dislocations, decreases in dislocation mobility and macroscopic hardening may be expected as the atmospheres provide a drag force. At some what higher temperatures, serrated yielding (Portevin - LeChatalier effect) can be expected and has been observed [48]. Increases in dislocation mobility due to H shielding are expected at each strain rate above the temperature of serrated yielding, as it is in this temperature and strain rate range that the H atmospheres can move with the dislocations and rearrange themselves to provide maximum shielding of the elastic interactions. It is this intermediate temperature range, in which H enhanced dislocation mobility is expected, that corresponds to the temperature range in which H embrittlement due to solute H is generally observed.

The reduction of barriers to dislocation motion by the presence of H in solid solution has been demonstrated using *in situ* environmental cell TEM measurements in many bcc, fcc. and hcp pure materials, solid solutions and precipitation hardened systems, in a few systems using macroscopic deformation, and in one system using thermal activation deformation methods. The theory of H shielding of elastic stress centers discussed above supports the increases in dislocation mobility due to the presence of H in solid solution. Due to the constraints of the observational systems, the *in situ* TEM measurements correspond to relatively low dislocation velocities (of the order of 10^{-4} to 10^{-6} m/sec) and hence to low stresses. To date they have been carried out only at about 290 K, and at this temperature the H shielding calculations support H enhanced dislocation velocities; as do the thermally activated deformation studies carried out on macroscopic specimens.

While some macroscopic deformation observations can be considered as supportive of the direct observations of H enhanced dislocation mobility, in many similar measurements, flow stress hardening rather than softening is observed. Several reasons may account for this dichotomy.

a. Many of the macroscopic deformation measurements which exhibit hardening on the introduction of H have been carried out at relatively high strain rates and at temperatures where the lagging of the H atmospheres behind the moving dislocations cause increases in the flow stress.

b. As discussed above, H induced slip localization can cause increases in the measured flow stress in experiments under imposed strain rates; even under conditions where the dislocation mobility is increased by the solute H.

c. Damage to the material during the introduction of H by high fugacity charging can result from very large H concentration gradients which cause stress gradients during charging. While small amounts of dislocation damage can cause softening due to introduction of dislocation sources, in general the large near surface deformations cause hardening of the material. This is particularly true in cases such as Ni where surface hydrides can form during cathodic charging.

CONCLUSIONS

In view of the complexity of H effects in the deformation and fracture of solids, no firm conclusions about the mechanism(s) of hydrogen related fracture can yet be reached. The evidence for fracture due to stress induced hydrides under conditions where hydrides are stable under stress is incontrovertible. Less firm conclusions can be reached for systems which do not exhibit hydride formation.

In non-hydride forming systems, the evidence for failure by Hydrogen Enhanced Local Plasticity is strong, based on microscopic observations of crack tip behavior and fracture surfaces. Strong evidence for H enhanced dislocation mobility has been obtained using *in situ* TEM studies, macroscopic stress strain curves, measurements of thermally activated dislocation motion, and theoretical treatments of hydrogen shielding of elastic stress centers.

Possible explanations for the "mixed" observations of hydrogen caused softening and hardening in macroscopic flow stress measurements have been advanced on the basis of damage caused by charging and slip localization. Hydrogen caused slip localization can result in increases in the macroscopic flow stress despite enhanced dislocation mobility.

REFERENCES

1. D. G. Westlake, *Trans. ASM 62* (1969) 1000.
2. H. K. Birnbaum, M. Grossbeck and S. Gahr, in I. M. Bernstein and A. W. Thompson (eds.), *Hydrogen in Metals,,* ASM Metals Park, Ohio, 1973, p. 303.
3. S. Gahr, M. L. Grossbeck and H. K. Birnbaum, *Acta Metall., 25* (1977) 1775.
4. D. Shih, I. M. Robertson and H. K. Birnbaum, *Acta Metall., 36* (1988) 111.
5. C. D. Beachem, *Metall. Trans., 3* (1972) 437.
6. H. K. Birnbaum, in R. P. Gangloff and M. B. Ives (eds), *Environment-Induced Cracking of Metals,* Houston, N.A.C.E. 1988, p. 21.
7. S. M. Meyers et al, *Reviews of Modern Physics, 64* (1992) 559.
8. E. Sirois, P. Sofronis, H. K. Birnbaum, in S. M. Bruemmer, et al. (eds.), *Fundamental Aspects of Stress Corrosion Cracking,* The Minerals, Metals and Materials Society, New York, 1992, p. 173.

9. H. K. Birnbaum, in N. Moody and A. W. Thompson (eds.), *Hydrogen Effects on Materials Behavior*, The Minerals, Metals and Materials Society, New York, 1990, p. 639.
10. E. A. Steigerwald, F. W. Schaller and A. R. Troiano, *Trans. Metall. Soc. AIME 218* (1960) 832.
11. R. A. Oriani and P. H. Josephic, *Acta Metall., 22* (1974) 1065.
12. D. H. Sherman, C. V. Owen and T. E. Scott, *Trans. AIME, 242* (1968) 1775.
13. M. L. Grossbeck and H. K. Birnbaum, *Acta Metall., 25* (1977) 125.
14. D. Hardie and P. McIntyre, *Metall. Trans., 4* (1973) 124.
15. N. E. Paton and J. C. Williams, in I. M. Bernstein and A. W. Thompson (eds.), *Hydrogen in Metals*, ASM, Metals Park, Ohio, 1973, p. 409.
16. K. Nuttall, in A. W. Thompson and I. M. Bernstein (eds.), *Effects of Hydrogen on the Behavior of Materials*, TMS, New York, 1975, p. 441.
17. S. Takano and T. Suzuki, *Acta Metall., 22* (1974) 265.
18. T. B. Flannagan, N. B. Mason and H. K. Birnbaum, *Scripta Metall., 14* (1981) 109.
19. T. Tabata and H. K. Birnbaum, *Scripta Metall., 18* (1984) 231.
20. I. M. Robertson and H. K. Birnbaum, *Acta Metall., 34* (1986) 353.
21. G. Bond, I. M. Robertson and H. K. Birnbaum, *Acta Metall., 36* (1988) 2193.
22. G. Bond, I. M. Robertson and H. K. Birnbaum, *Acta Metall., 35* (1988) 2289.
23. P. Rozenak, I. M. Robertson and H. K. Birnbaum, *Acta Metall., 38* (1990) 2031.
24. T. Tabata and H. K. Birnbaum, *Scripta Metall., 187* (1984) 947.
25. J. Eastman, T. Matsumoto, N. Narita, F. Heubaum and H. K. Birnbaum, in I. M. Bernstein and A. W. Thompson (eds.), *Hydrogen in Metals*, TMS, New York, 1980, p. 397.
26. M. S. Daw and M. I. Baskes, *Phys. Rev., B 29* (1984) 6443.
27. J. P. Hirth and J. R. Rice, *Metall. Trans., A, 11* (1980) 1501.
28. J. P. Hirth, *Phil. Trans. Royal Soc. Lon., Ser. A 295* (1980) 139.
29. T. Matsumoto, J. Eastman and H. K. Birnbaum, *Scripta Metall., 15* (1981) 1033.
30. H. Z. Xiao, Ph.D. Thesis. University of Illinois (1993).
31. H. Hanninen, T. C. Lee, I. M. Robertson, and H. K. Birnbaum, Proc. of Int. Conf. on Corrosion - Deformation Interactions (1992) In press
32. H. Fukushima and H. K. Birnbaum, *Acta Metall., 32* (1984) 851.
33. D. Lassila and H. K. Birnbaum, *Acta Metall., 34* (1986) 1237.
34. D. Lassila and H. K. Birnbaum, *Acta Metall., 35* (1987) 1815.
35. I. M. Robertson, T. Tabata, W. Wei, F. Heubaum and H. K. Birnbaum, *Scripta Metall., 18* (1984) 841.
36. H. Matsui, H. Kimura and S. Moriya, *Mat. Sci. Eng., 40* (1979) 207.
37. S. Moriya, H. Matsui and H. Kimura, *Mat. Sci. Eng., 40* (1979) 217.
38. H. Matsui, H. Kimura and A. Kimura, *Mat. Sci. Eng., 40* (1979) 227.
39. F. Zeides, Ph.D. Thesis. University of Illinois (1986).
40. E. Sirois, Ph.D. Thesis. University of Illinois (1992).
41. D. G. Ulmer and C. J. Altstetter, *Acta Metall., 28* (1991) 1237
42. W. A. McInteer, A. W. Thompson and I. M. Bernstein, *Acta Metall., 28* (1980) 887
43. E. Sirois and H. K. Birnbaum, to be published.
44. J. P. Hirth and B. Carnahan, *Acta Metall., 26* (1978) 1795.

45. P. Sofronis and H. K. Birnbaum, *J. Mech. Phys. Solids*, submitted.
46. A. W. Cochardt, G. Schoeck, and H. Wiedersich, *Acta. Metall., 3* (1955) 533.
47. A. N. Stroh, *Adv. Phys., 6* (1957) 418.
48. A. Kimura and H. K. Birnbaum *Acta Metall. Mater., 38* (1990) 1343.

ACKNOWLEDGMENTS

This work was supported by the Department of Energy under grant DEFG02-91ER45439.

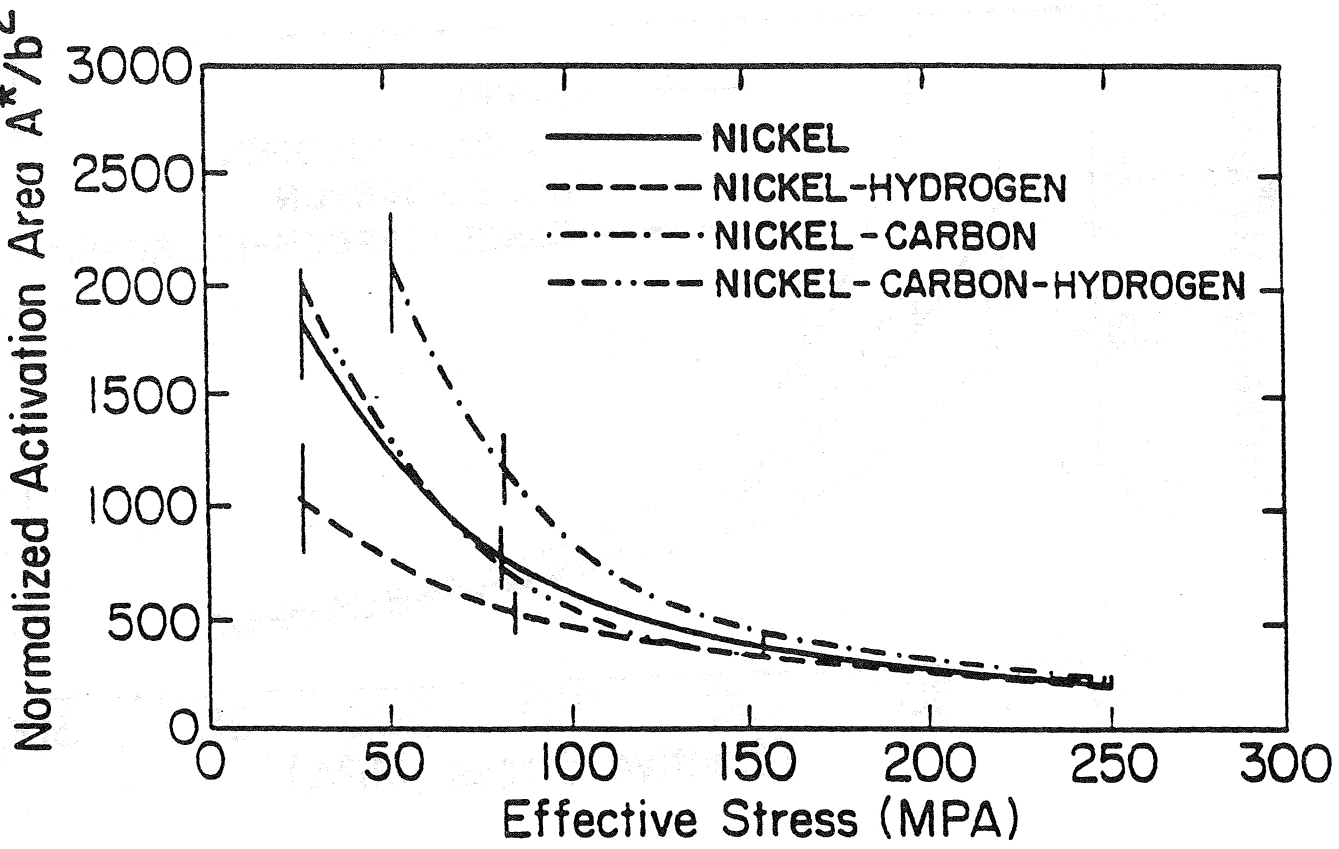

Fig. 1 Effects of alloy composition on the dependence of the activation area, A^*, on the effective stress, σ^*. Pure Ni ——— ; Ni-H - - - - ; Ni-C — · — · — ; Ni-C-H - - ·· - - ·· - - ·· - - .

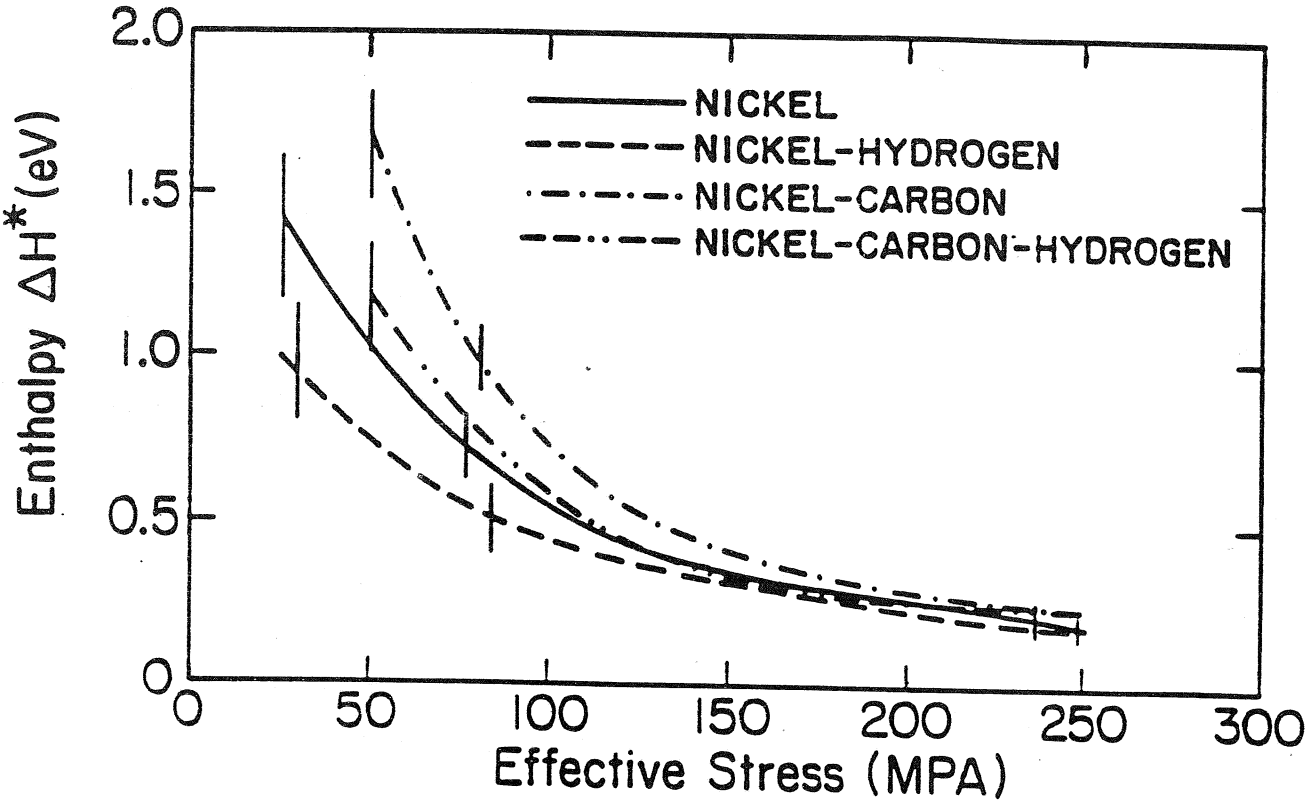

Fig. 2 Effects of alloy composition on the dependence of the activation enthalpy, ΔH^*, on the effective stress, σ^*. Pure Ni ———— ; Ni-H - - - - - - - - ; Ni-C — · — · — · ; Ni-C-H - - ·· - - ·· - - ·· - - .

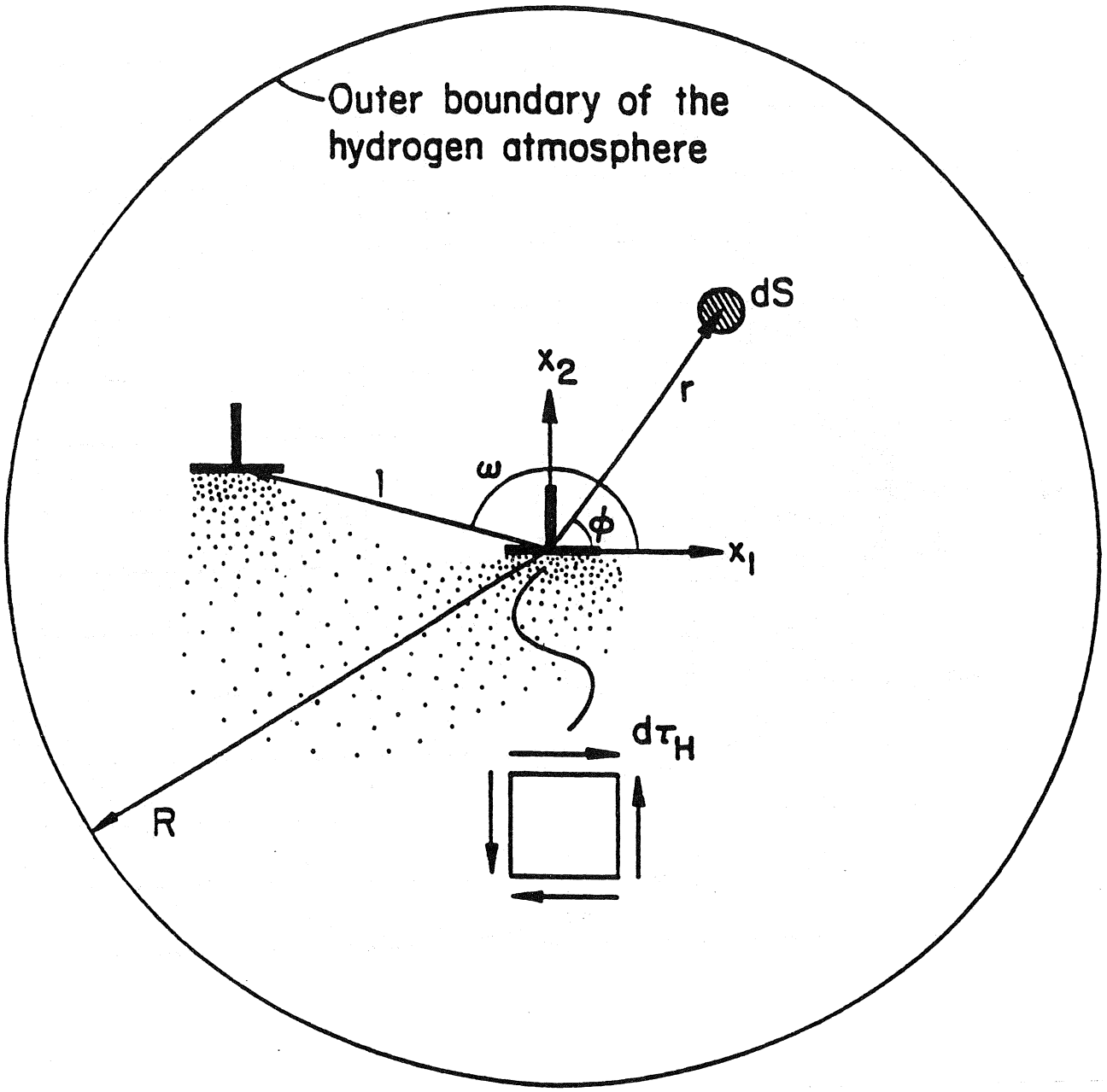

Fig. 3 Schematic showing the coordinates of the interacting dislocations and the hydrogen atmospheres. The shear stress, $d\tau_H$ is the shear stress due to the hydrogen atmosphere in the area dS located at position (r,ϕ). The extent of the outer radius of the H atmosphere, R, is determined by convergence of the full elastic solutions.

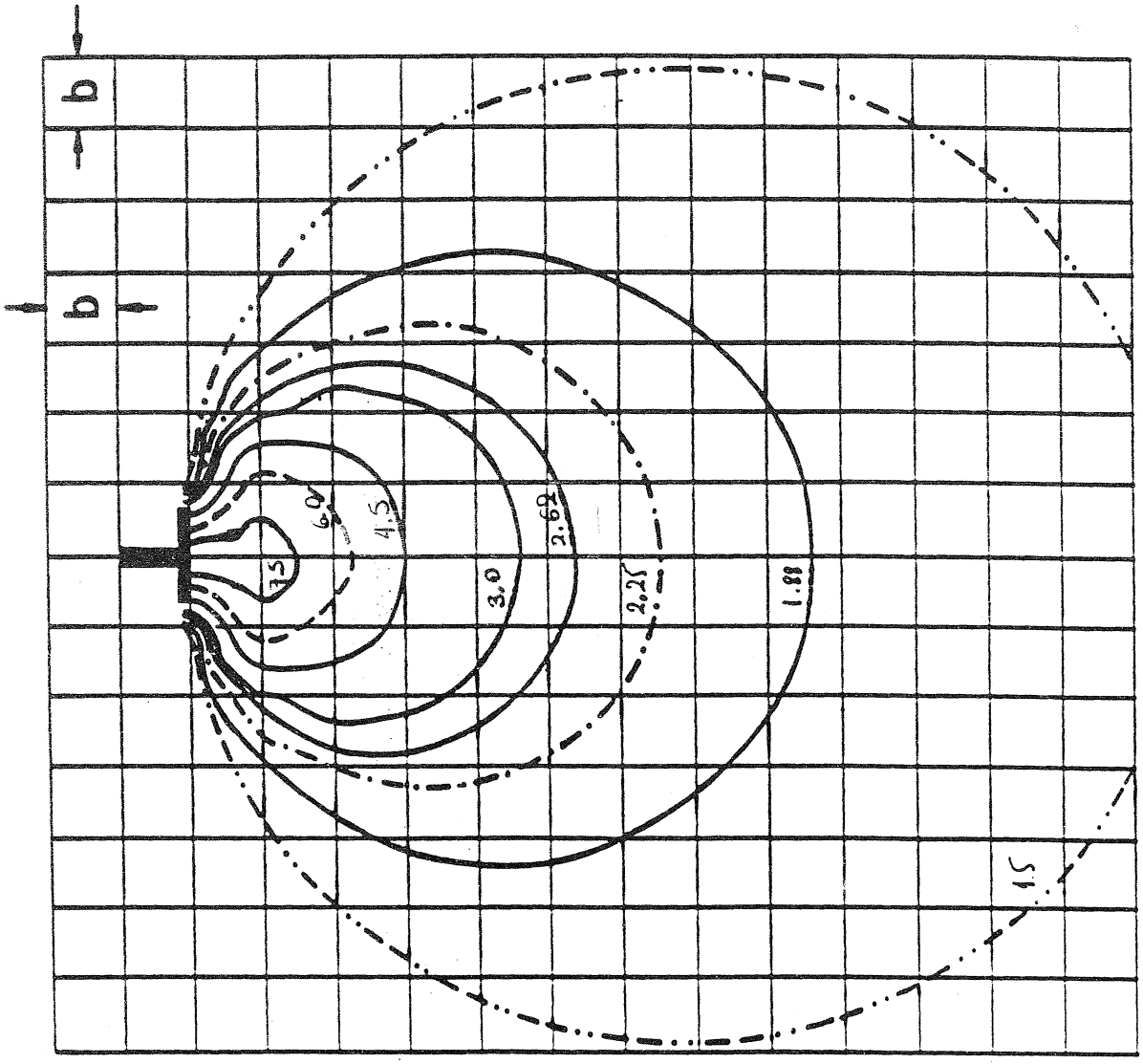

Fig. 4 Isoconcentration contours of the normalized hydrogen concentration, C/C_o, around an isolated edge dislocation. Calculations are for the parameters of Nb containing $C_o = 0.1$ (H/M = 0.1) at 300 K. $C/C_o = 6$ - - - - - - ; $C/C_o = 2.25$ - · - · - · ; $C/C_o = 1.5$ - - ·· - - ·· - - .

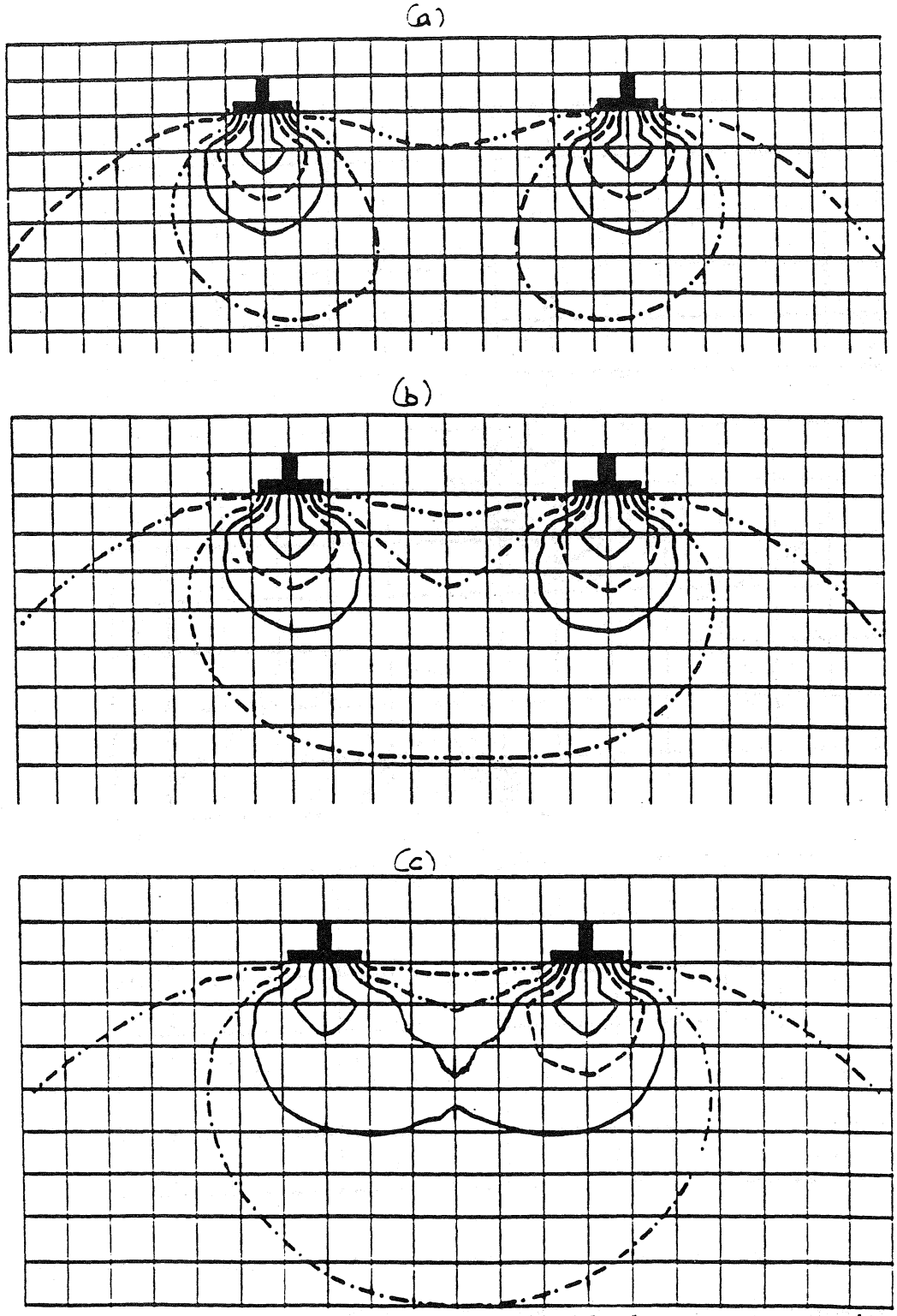

Fig. 5 Isoconcentration contours of the normalized hydrogen concentration, C/C_o, around two parallel edge dislocations having equal Burgers vectors of magnitude, b, on the same slip plane. Calculations are for the parameters of Nb containing $C_o = 0.1$ (H/M = 0.1) at 300 K. a) dislocation distance 10b, b) dislocation distance 8b, c) dislocation distance 6b. $C/C_o = 6$ - - - - - -;

$C / C_o = 3$ - · - · - · - ; $C / C_o = 1.5$ - - ·· - - ·· - - .

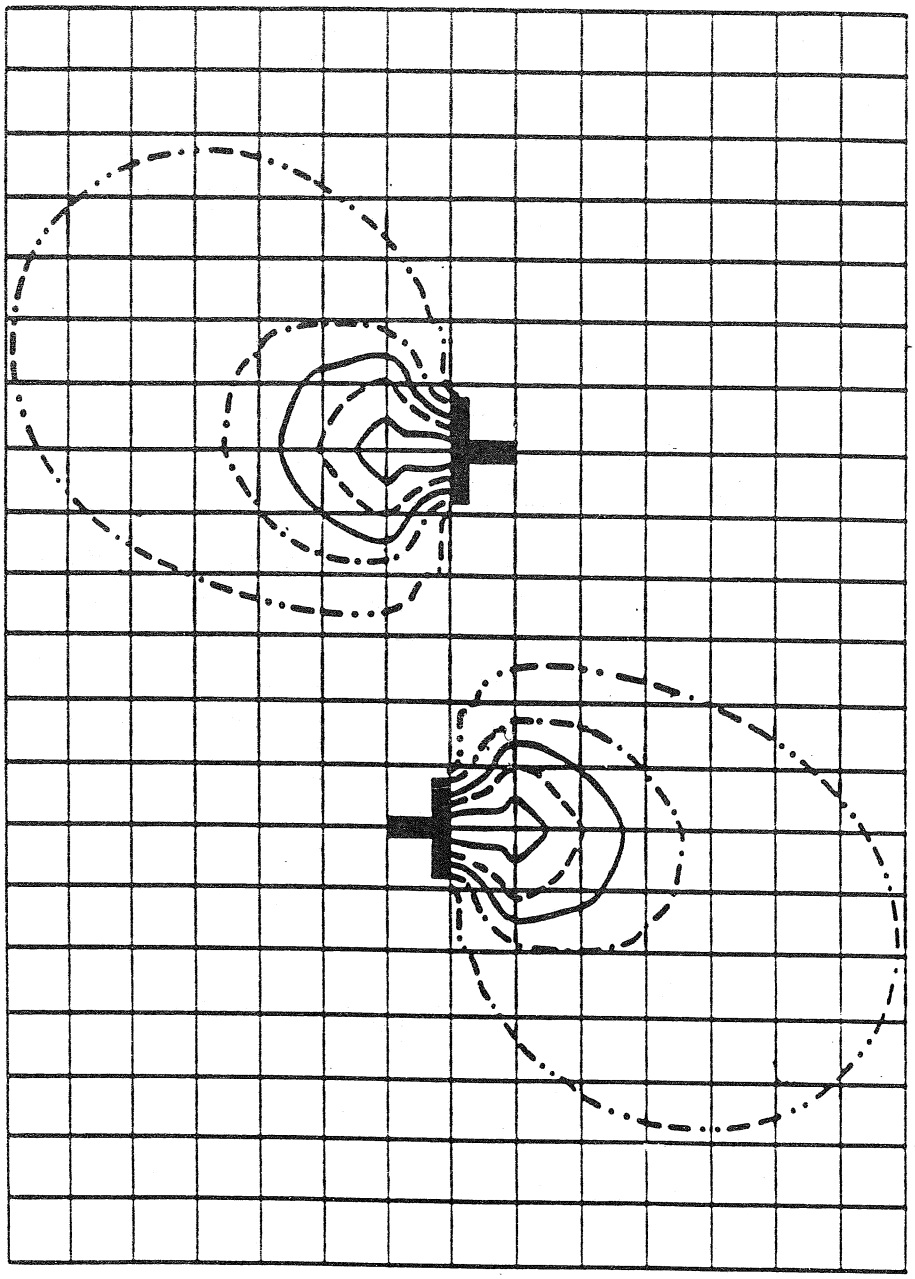

Fig. 6 Isoconcentration contours of the normalized hydrogen concentration, C/C_o, around two parallel edge dislocations having opposite Burgers vectors of magnitude, b, on the same slip plane. Calculations are for the parameters of Nb containing $C_o = 0.1$ (H/M = 0.1) at 300 K. a) dislocation distance 10b, b) dislocation distance 8b, c) dislocation distance 6b. $C/C_o = 6$ - - - - ; $C/C_o = 3$ - · - · - · - ; $C/C_o = 1.5$ - - ·· - - ·· - - .

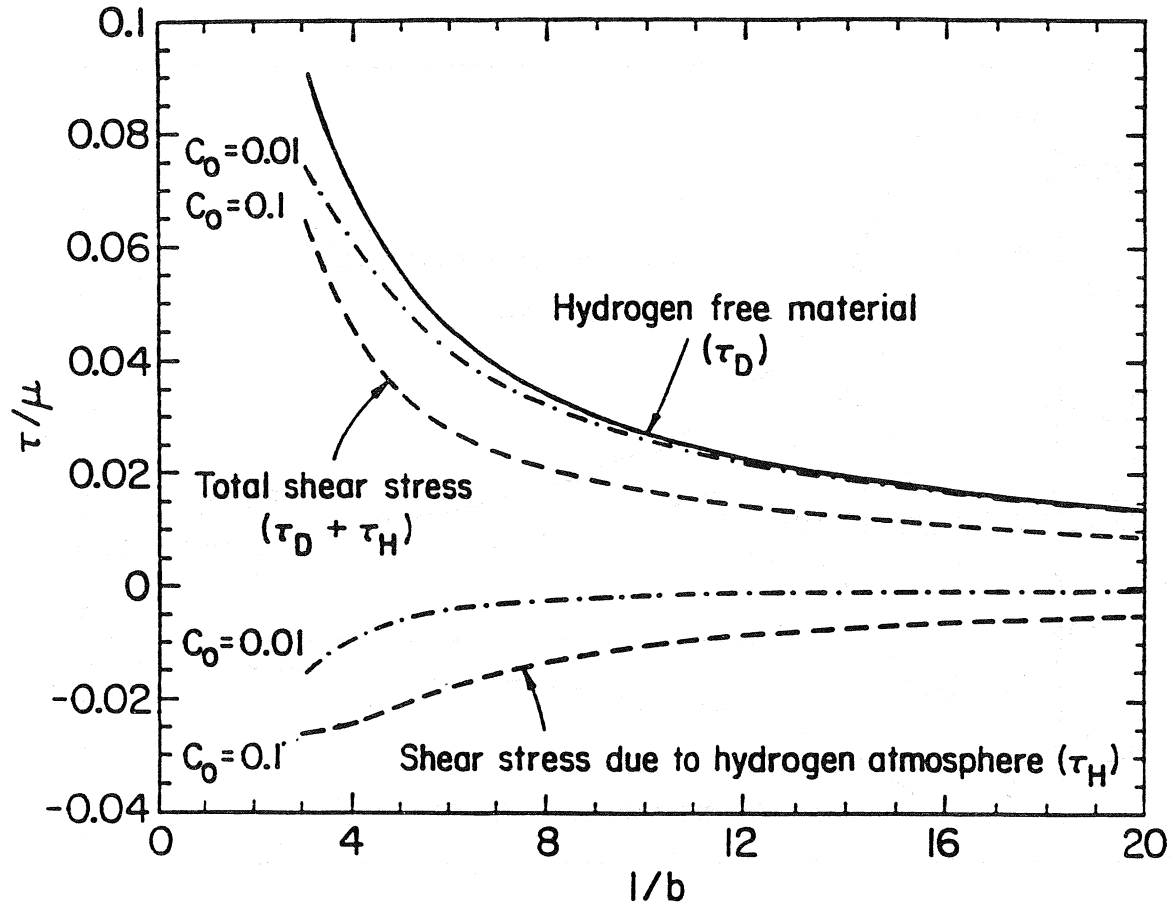

Fig. 7 Plots of the normalized shear stresses on dislocation 2, τ_H / μ due to H, τ_D / μ due to dislocation 1, and the net shear stress $(\tau_D + \tau_H) / \mu$ vs. normalized distance along the slip plane, l/b, for parallel edge dislocations having equal Burgers vectors. Calculations were carried out for the parameters characteristic of Nb at 300 K. Hydrogen free material ——— ; H/M = 0.01 - · - · - · - ; H/M = 0.1 - - - - - - .

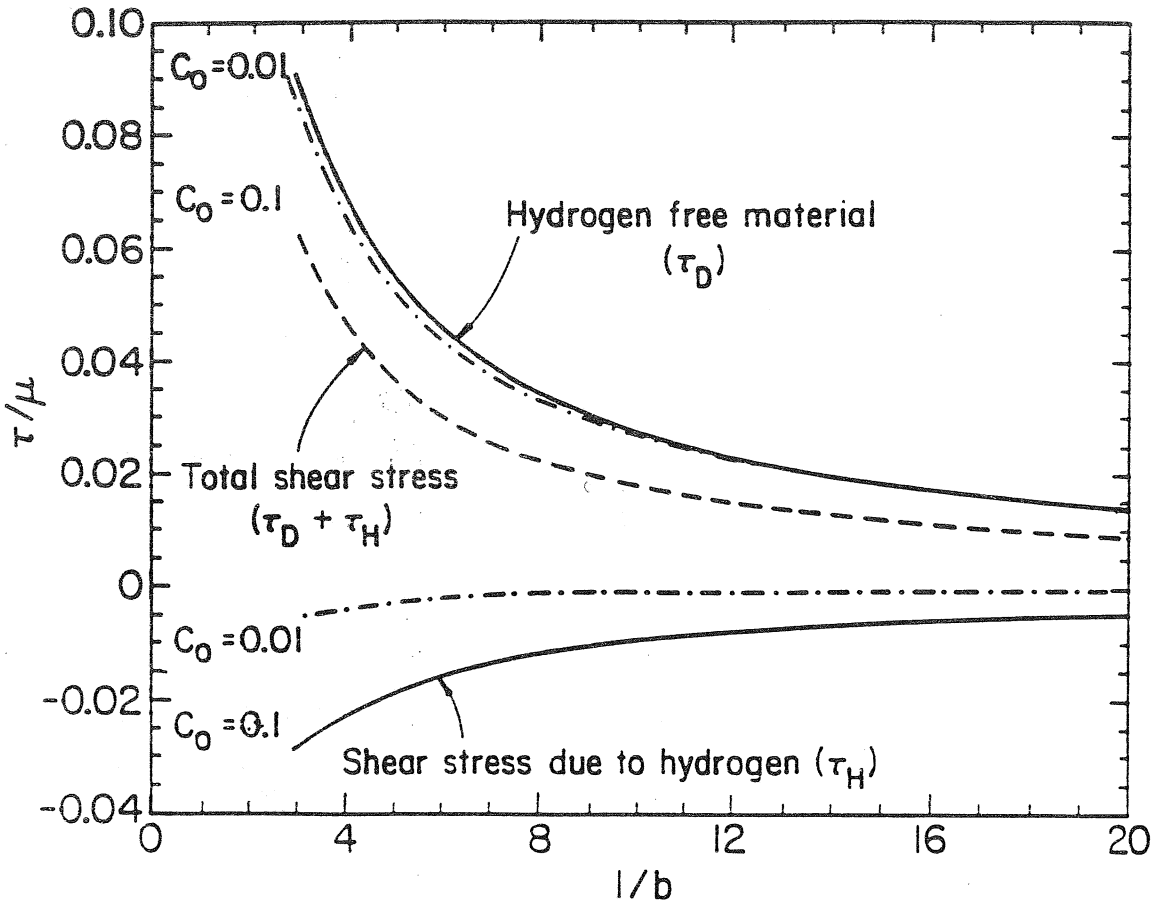

Fig. 8 Plots of the normalized shear stresses on dislocation 2, τ_H / μ due to H, τ_D / μ due to dislocation 1, and the net shear stress $(\tau_D + \tau_H) / \mu$ vs. normalized distance along the slip plane, 1/b, for parallel edge dislocations having opposite Burgers vectors. Calculations were carried out for the parameters characteristic of Nb at 300 K. Hydrogen free material ——— ; H/M = 0.01 - · - · - · - ; H/M = 0.1 - - - - - - .

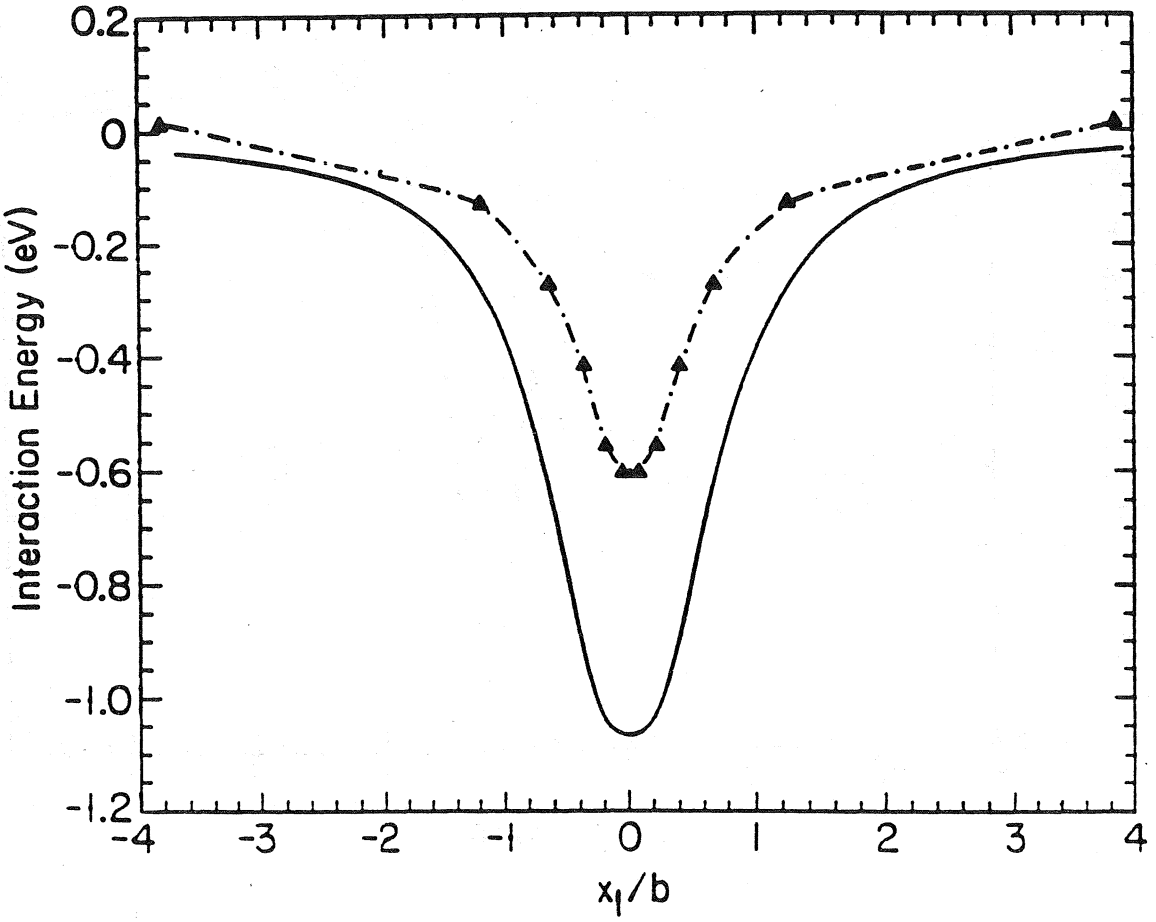

Fig. 9 Plot of the interaction energy, W, between an edge dislocation and a C interstitial solute having a tetragonal axis along the [100] as a function of the normalized distance along the slip plane, x_1/b. The C solute is located at a distance x_2/b = -0.505. The calculation was carried out for the parameters of Nb at 300 K. H/M = 0 (pure Nb) ———— ; H/M = 0.1 — · — · — .

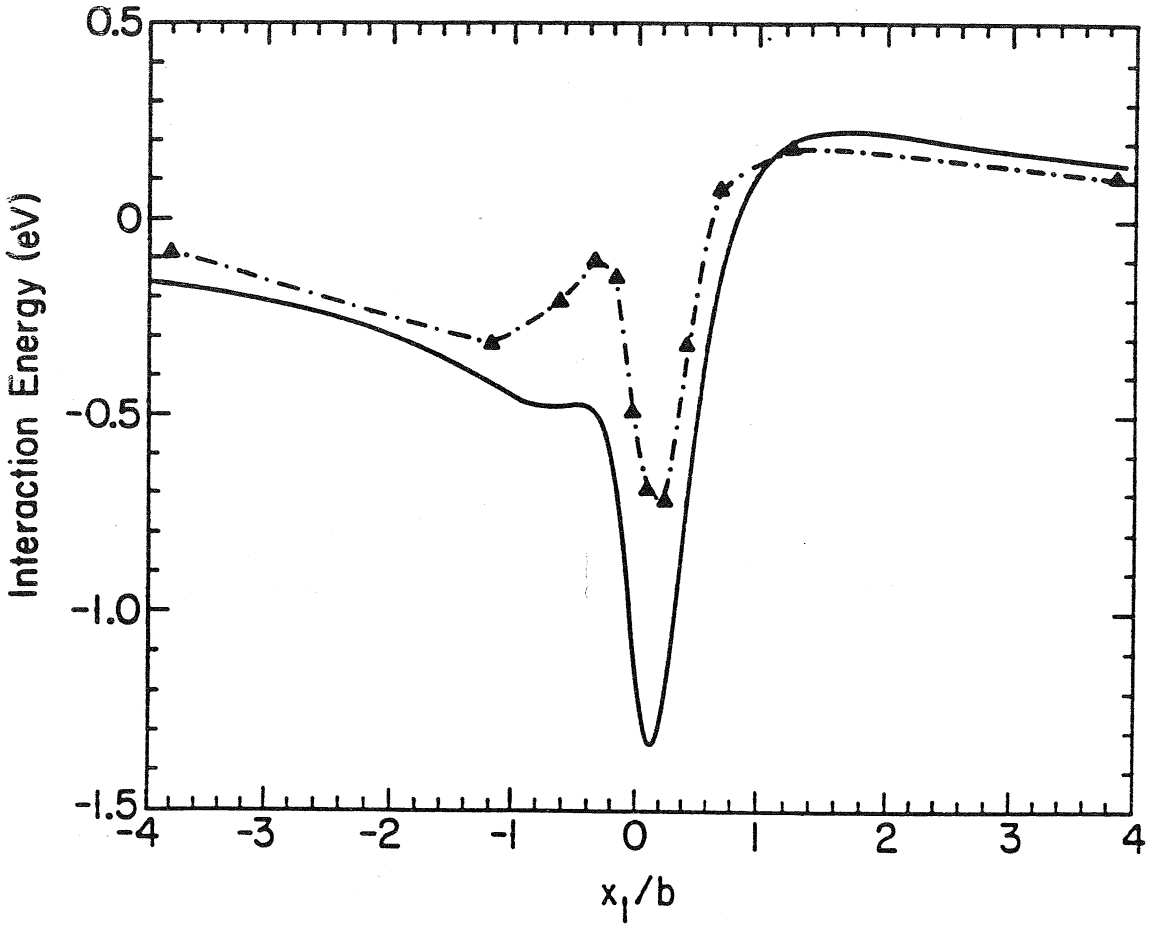

Fig. 10 Plot of the interaction energy, W, between an edge dislocation and a C interstitial solute having a tetragonal axis along the [010] as a function of the normalized distance along the slip plane, x_1/b. The C solute is located at a distance x_2/b = -0.505. The calculation was carried out for the parameters of Nb at 300 K. H/M = 0 (pure Nb) ———— ; H/M = 0.1 — · — · — .

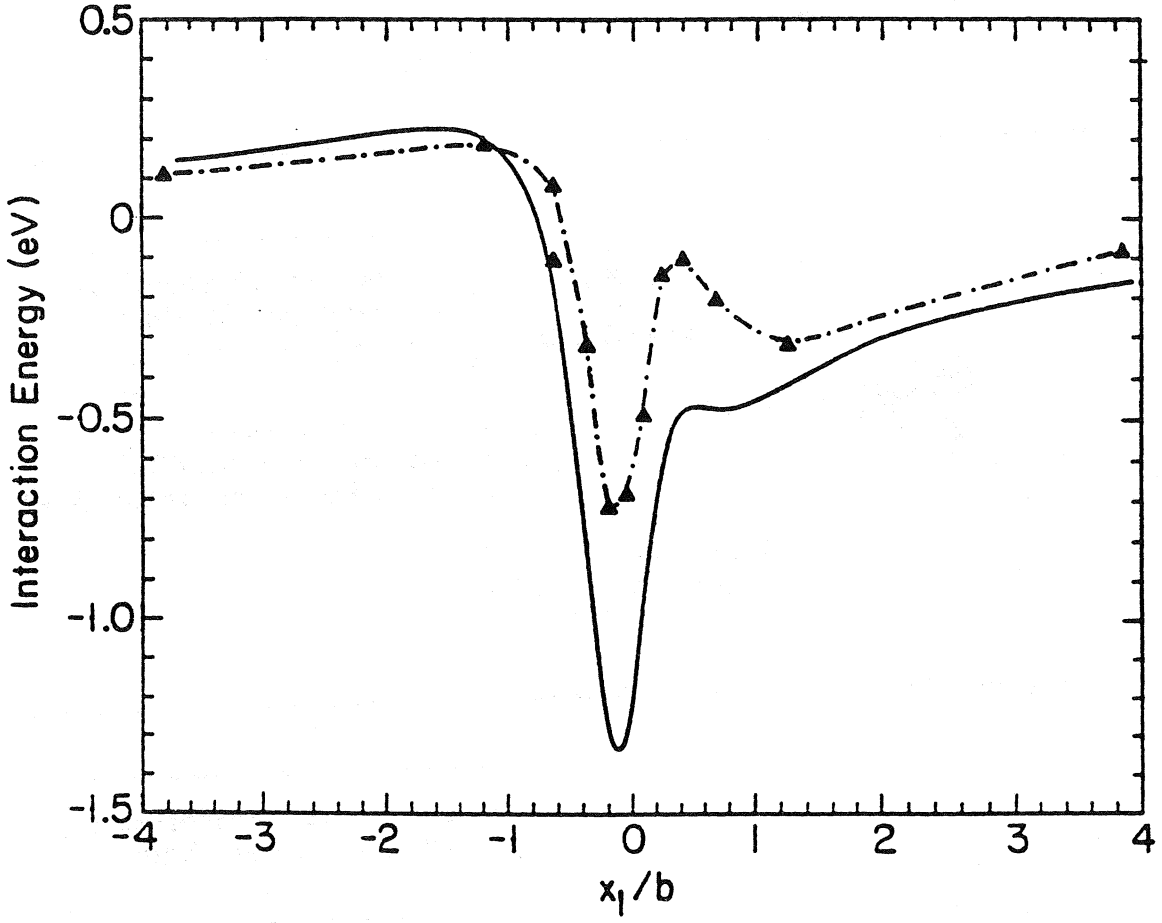

Fig. 11 Plot of the interaction energy, W, between an edge dislocation and a C interstitial solute having a tetragonal axis along the [001] as a function of the normalized distance along the slip plane, x_1/b. The C solute is located at a distance x_2/b = -0.505. The calculation was carried out for the parameters of Nb at 300 K. H/M = 0 (pure Nb) ———— ; H/M = 0.1 — · — · — .

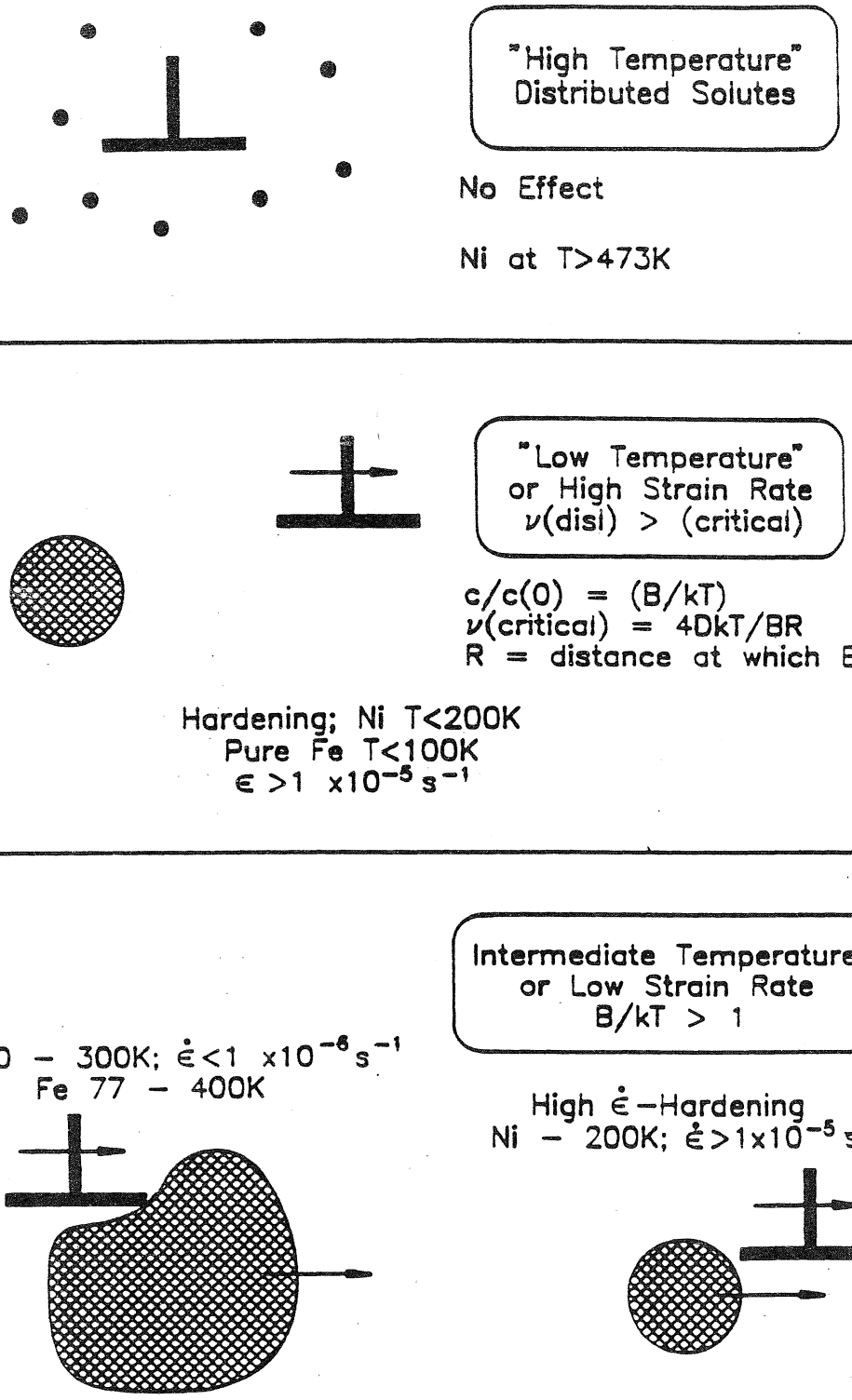

Fig. 12 Schematic diagram showing the effects of the elastic shielding by hydrogen at various temperatures and strain rates.

List of Recent TAM Reports

No.	*Authors*	*Title*	*Date*
489	Shawki, T. G.	Necessary and sufficient conditions for the onset of shear strain localization in thermal viscoplastic materials	Dec. 1988
490	Dasgupta, A.	An experimental investigation of homogeneous fatigue damage in a random short-fiber composite under combined tension-torsion loading	Dec. 1988
491	Lee, H.-I., and D. S. Stewart	Calculation of linear detonation instability--Part I: One-dimensional instability of plane detonation	Dec. 1988
492	Weaver, R. L.	Diffusivity of ultrasound in polycrystals	Feb. 1989
493	Shawki, T. G., R. J. Clifton, and Y. Kadioglu	Calculation of the viscoplastic response of polycrystals from slip theory for FCC single crystals	Mar. 1989
494	Toro, J. R.	Existence of weak solutions to the thick plate problem with various boundary conditions	Apr. 1989
495	Stewart, D. S., and B. W. Asay	Discrete modeling of beds of propellant exposed to strong stimulus	Apr. 1991
496	Klein, R., and D. S. Stewart	The relation between curvature, rate state dependence, and detonation velocity	Apr. 1991
497	Powers, J. M., and D. S. Stewart	Approximate solutions for oblique detonations in the hypersonic limit	Apr. 1991
498	Davidson, M. T., K. L. Kuster, K. W. Quinn, N. A. Sluz, and G. Stojkovich	Twenty-fifth student symposium on engineering mechanics, M. E. Clark, coord. (1988)	Feb. 1992
499	Cardenas, H. E., W. C. Crone, D. J. Scott, G. G. Stewart, and B. F. Tatting	Twenty-sixth student symposium on engineering mechanics, M. E. Clark, coord. (1989)	Mar. 1992
700	Juister, C. E., D. W. Newport, C. S. Payne, J. M. Peters, M. P. Thomas, and J. C. Trovillion	Twenty-seventh student symposium on engineering mechanics, M. E. Clark, coord. (1990)	Apr. 1992
701	Bernard, R. T., D. W. Claxon, J. A. Jones, V. R. Nitzsche, and M. T. Stadtherr	Twenty-eighth student symposium on engineering mechanics, M. E. Clark, coord. (1991)	Apr. 1992
702	Greening, L. E., P. J. Joyce, S. G. Martensen, M. D. Morley, J. M. Ockers, M. D. Taylor, and P. J. Walsh	Twenty-ninth student symposium on engineering mechanics, J. W. Phillips, coord. (1992)	May 1992
703	Kuah, H. T., and D. N. Riahi	Instabilities and transition to chaos in plane wakes	Nov. 1992
704	Stewart, D. S., K. Prasad, and B. W. Asay	Simplified modeling of transition to detonation in porous energetic materials	Nov. 1992
705	Stewart, D. S., and J. B. Bdzil	Asymptotics and multi-scale simulation in a numerical combustion laboratory	Jan. 1993
706	Hsia, K. J., Y.-B. Xin, and L. Lin	Numerical simulation of semi-crystalline Nylon 6: Elastic constants of crystalline and amorphous parts	Jan. 1993
707	Hsia, K. J., and J. Q. Huang	Curvature effects on compressive failure strength of long fiber composite laminates	Jan. 1993
708	Jog, C. S., R. B. Haber, and M. P. Bendsoe	Topology design with optimized, self-adaptive materials	Mar. 1993
709	Barkey, M. E., D. F. Socie, and K. J. Hsia	A yield surface approach to the estimation of notch strains for proportional and nonproportional cyclic loading	Apr. 1993
710	Feldsien, T. M., A. D. Friend, G. S. Gehner, T. D. McCoy, K. V. Remmert, D. L. Riedl, P. L. Scheiberle, and J. W. Wu	Thirtieth student symposium on engineering mechanics, J. W. Phillips, coord. (1993)	Apr. 1993
711	Weaver, R. L.	Anderson localization in the time domain: Numerical studies of waves in two-dimensional disordered media	Apr. 1993
712	Cherukuri, H. P., and T. G. Shawki	An energy-based localization theory	Apr. 1993
713	Manring, N. D., and R. E. Johnson	Modeling a variable-displacement pump	June 1993
714	Birnbaum, H. K., and P. Sofronis	Hydrogen-enhanced localized plasticity—A mechanism for hydrogen-related fracture	July 1993